Modelling of a narrow linewidth monolithically integrated quantum dot-on-silicon extended cavity laser

Christina Vivian[a], James Seddon[a], Ilias Skandalos[b], Mingchu Tang[a], Frederic Y. Gardes[b], Huiyun Liu[a], and Alwyn J. Seeds[a]

[a]Electronic and Electrical Engineering Dept., University College London, London WC1E 7JE, United Kingdom
[b]Optoelectronics Research Centre, University of Southampton, University Road, Southampton, United Kingdom

ABSTRACT

This work reports on the modelling of an on-chip extended cavity laser (ECL) formed of III/V quantum dots (QDs) monolithically grown on silicon and integrated with a silicon nitride waveguide layer which contains a second-order, surface-etched Bragg grating. A coupling coefficient of 47 cm^{-1} was extracted from full-wave simulations in CST Studio Suite. Combining this with measurements from a Fabry-Perot QD laser predicts a spectral linewidth for the proposed three-section ECL as low as 17 kHz. This is an order of magnitude smaller than commercial O-band lasers, highlighting the capabilities of QDs directly grown on silicon for advancing silicon photonic systems that require high coherence.

Keywords: Quantum dots, extended cavity laser, silicon nitride, silicon photonics, monolithic integration

1. INTRODUCTION

Significant progress has been made in direct growth techniques of III/V semiconductor quantum dots (QDs) on silicon substrates[1] such as through focused efforts towards CMOS-compatible fabrication processes[2] and mitigating performance-hindering defects including threading dislocations[3] and anti-phase boundaries.[4] This has been transformational for the development of monolithic integrated silicon photonics which, compared to its hybrid counterpart, promises a more cost-effective and scalable approach to producing complex optoelectronic and photonic integrated circuits (PICs) on a silicon platform.

As more applications seek out the benefits of photonic integration such as size, weight, power and lower losses, the desire for reliable yet versatile building blocks grows along with interest in directly interfacing these with existing PIC technologies such as silicon on insulator (SOI) and silicon nitride (SiN). These platforms are known to have low propagation and bending losses, allowing for small device footprints. Silicon nitride also has the advantage of a large transparency window (400 nm - 7 μm)[5] making it practical for a wide variety of applications and those which operate over a large span of wavelengths.

Recent work outlining an interfacing strategy between III/V QD-SiN[6] has demonstrated the feasibility of integrating the III/V QD optical gain material with versatile SiN for passive circuitry. In this work, we propose a monolithically integrated narrow-linewidth extended cavity laser (ECL) following this fabrication scheme. The design process of creating this device, particularly the second-order Bragg grating needed for filtering out higher longitudinal cavity modes, and a numerical model for estimating the spectral linewidth is presented. A narrow-linewidth integrated laser is necessary for systems which demand low phase noise such as a coherent, high-speed data transceiver as well as for sources which require a long coherence length.

Further author information: (Send correspondence to Christina Vivian)
E-mail: christina.vivian.20@ucl.ac.uk

Silicon Photonics XX, edited by Graham T. Reed, Jonathan Bradley,
Proc. of SPIE Vol. 13371, 133710P · © 2025 SPIE
0277-786X · doi: 10.1117/12.3042230

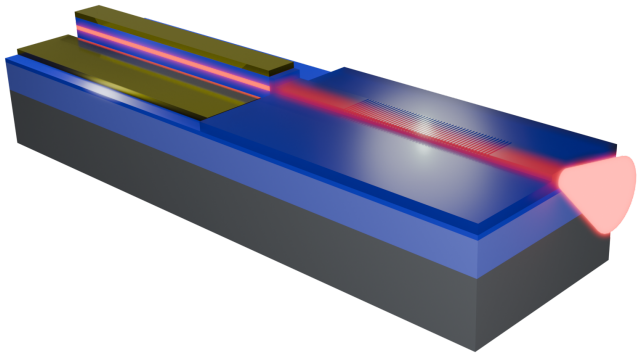

Figure 1. Conceptual schematic of the III/V-on-Si extended cavity laser with SiN passive elements.

2. EXTENDED CAVITY LASER DESIGN AND MODEL

The conceptualization of the proposed ECL is shown in Figure 1 which consists of three key sections of the device. Namely, these are the InAs QD active, straight SiN waveguide and SiN Bragg grating sections. A twin-chamber molecular beam epitaxy system is used to deposit a 500 nm thick Ge-on-Si virtual substrate on silicon before growing a 7-layer InAs quantum dot-in-well stack.[7] This is integrated with a micrometre-scale N-rich SiN rib waveguide platform[5] (1.6 μm thick and 1.7 μm wide rib for single-mode propagation)[6] which has been optimised to passivate the higher index III/V material as well as minimize coupling losses and back-reflections at the interface. The N-rich SiN waveguide will be grown using plasma enhanced chemical vapour deposition and the grating corrugations fabricated by electron beam lithography which is followed by a silicon dioxide top cladding.

2.1 Bragg Grating Design

The simplest of Bragg grating, a rectangular surface-etched design as shown in Figure 2, was chosen for a first demonstration of the integrated III/V QD-SiN technology. The specification for this grating is guided by the desired spectral characteristics of the laser which includes stable single-mode emission of a wavelength, λ around 1300 nm with a narrow linewidth and large side-mode suppression ratio for intended use in O-band systems. The

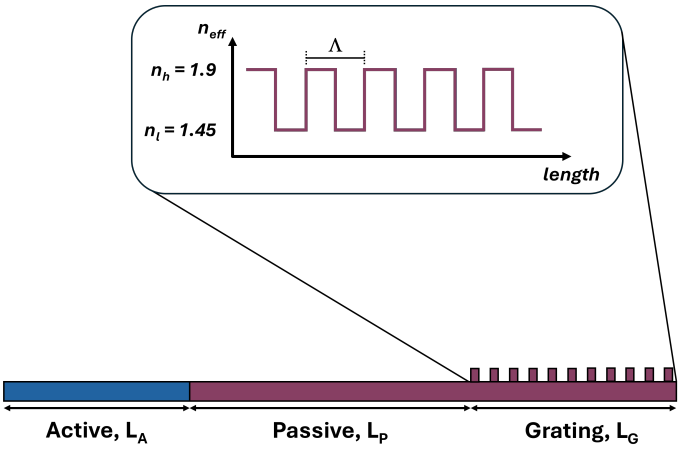

Figure 2. Simplified three-section model of the extended cavity. Inset shows the rectangular Bragg grating formed from high, n_h and low, n_l effective indices of 1.9 and 1.45 respectively and a pitch of Λ.

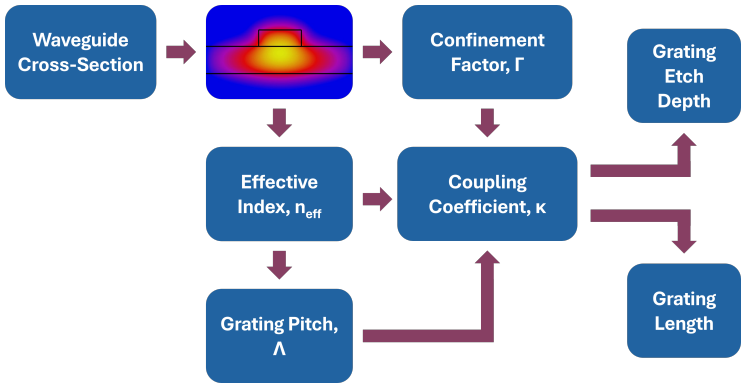

Figure 3. Design flow diagram used in this work to determine our second-order surface-etched Bragg grating specification. A simulated profile of the SiN rib waveguide fundamental TE mode is also shown.

design flow to determine key features of a second-order grating including the pitch, Λ, etching depth, expected coupling coefficient, κ and grating length, L is illustrated in Figure 3 for an assumed duty cycle. By first generating a 3D full-wave model of the SiN waveguide and corresponding unperturbed waveguide in CST Studio Suite, the simulated mode profiles were used to extract the effective index, n_{eff} and confinement factor, Γ for the fundamental TE mode respectively. For a narrow-area QD laser of 7 μm width, a SiN waveguide rib width of 6.17 μm is chosen for its optimised TE mode coupling losses and back-reflections at the interface, and large modal overlap between the two sections. An effective index of 1.867 for this waveguide cross-section results in a pitch of $\Lambda = 696$ nm using the Bragg condition:

$$m\lambda = 2n_{eff}\Lambda, \tag{1}$$

where m is the order number.

The coupling coefficient and the grating length jointly contribute to the Bragg grating reflectivity. Using modified coupled-mode equations[8] with full-wave modelling results, the coupling coefficient can be simplified to:

$$\kappa = \frac{(n_h^2 - n_l^2)\Gamma}{2n_{eff}^2\Lambda}\sin(m\pi D), \tag{2}$$

where D is the duty cycle. This value is also dependent on the grating tooth depth which, along with duty cycle, is reliant on the precision of the lithography tools used. For this reason, a duty cycle of 60% is chosen to avoid the practical challenge of etching very narrow teeth or gaps. Furthermore, an etch depth where κ stabilises is more reliable for predicting grating behaviour which is at $\kappa = 47$ cm^{-1} for an etch depth of 0.3 μm for this structure. Finally, also derived from coupled-mode theory, the length of the grating is related to the peak reflection, R_{peak} by:

$$R_{peak} = \tanh^2(\kappa L), \tag{3}$$

which gives the minimum grating length needed for a desired reflection maxima. For the more stable value of κ equal to 47 cm^{-1}, this translates to a grating length over 387 μm to achieve a reflection coefficient greater than 0.9, for example.

3. RESULTS AND DISCUSSION

A 3D full-wave model of the grating with the derived design parameters was then created in CST Studio to evaluate the reflection spectrum. These results are presented in Figure 4 for a fixed rib width of 6.17 μm over different lengths. With increasing length, the Bragg grating behaves increasingly selective at the desired wavelength therefore displaying strong side-mode suppression. For the longest modelled grating of 280 μm, the secondary wavelength peak at 1302 nm is weaker by almost a factor of 6 in this case.

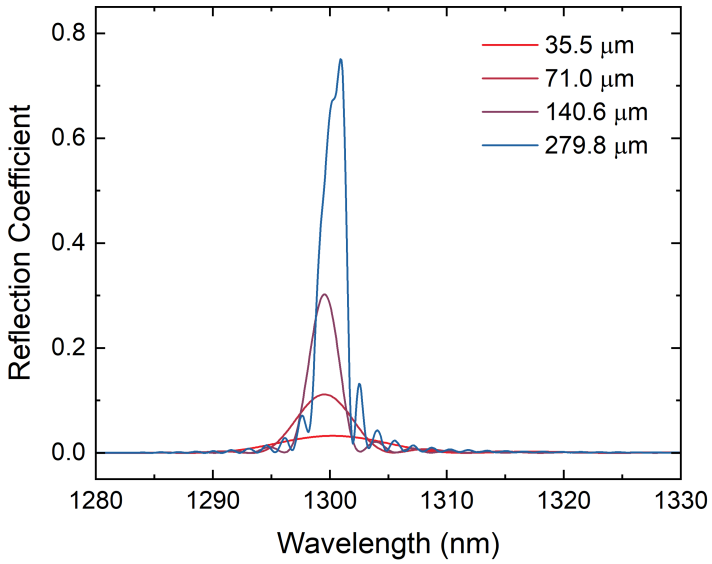

Figure 4. Simulated reflection response of second-order Bragg gratings with $\Lambda = 696$ nm, $D = 60\%$ and a fixed etch depth of 0.3 μm for various lengths.

3.1 Linewidth Estimation

The spectral linewidth, $\Delta\nu$ for the proposed ECL design was then estimated following a modified Schawlow-Townes approximation[9] combined with extracted experimental characterisation parameters of a Fabry-Perot (FP) QD laser. For a three-section model of the ECL with a QD active length, L_A and straight SiN passive length, L_P as depicted in Figure 2:

$$\Delta\nu = \frac{h\nu}{8\pi P}\left(\frac{L_A}{L_A + L_P + L_{Deff}}\right)^2 \nu_g^2(g_{th} - a_i)g_{th}n_{sp}(1+\alpha^2), \tag{4}$$

where $h\nu$ is the photon energy, P is the laser output power, ν_g is the group velocity, g_{th} is the threshold modal gain, a_i is the active region loss, n_{sp} is the spontaneous emission factor and L_{Deff} is the effective grating section length which accounts for the optical field penetration into the grating as well as waveguide propagation loss. For a given κ and fixed waveguide losses, this value will saturate for a long enough physical grating length. α is the linewidth enhancement factor; this quantifies the additional line broadening observed from laser dynamical effects, namely the change in refractive index due to a changing carrier density from spontaneous emission events.

The modal gain spectra and FP resonances in the amplified spontaneous emission spectra of InAs FP QD lasers were used to determine a_i and α which were 2 cm^{-1} and 1.2 respectively. The g_{th} was calculated from the cavity and mirror losses of the FP device as 33 cm^{-1}. These were fed into Equation 4 for a given active cavity length of $L_A = 2.5$ mm and a fixed physical grating length L_G of 868 μm as this is when L_{Deff} saturates at a value of 213 μm. These results are evaluated for different straight passive section lengths and are displayed in Figure 5. All iterations suggest a spectral linewidth < 100 kHz, with a minimum of $\Delta\nu = 17$ kHz observed for the longest calculated passive section length of 5 mm. Interestingly, Figure 5 suggests that an L_P of 1 mm predicts a value of $\Delta\nu$ slightly larger than a Fabry-Perot laser of the same active cavity length. This could suggest that the value of κ is not at its optimum as, if this is too small, the reflectivity of a grating for a given length will be too low. Equally if κ is too big, the effective grating length is too small which broadens $\Delta\nu$ in accordance to Equation 4.

4. CONCLUSION

This work has detailed the design process for a second-order SiN Bragg grating to be monolithically integrated with III/V QDs directly grown on silicon which forms an initial step towards demonstrating an O-band narrow-linewidth extended cavity laser for this novel silicon photonics platform. The calculated spectral linewidth of

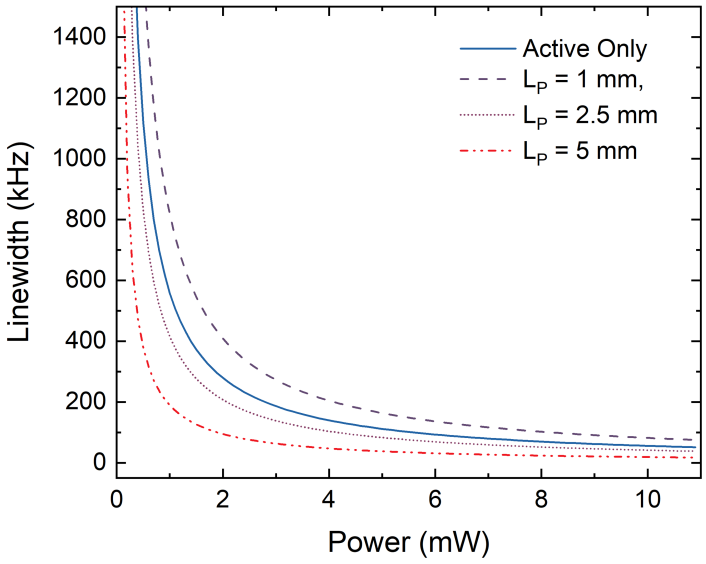

Figure 5. Calculated linewidth of extended cavity lasers with a fixed active and straight waveguide but varying grating lengths over a range of laser output powers.

such an ECL is predicted to be in the order of 10s of kHz, with a minimum linewidth calculated to be 17 kHz for a total device length of around 8.4 mm. Future work will focus on characterising the SiN Bragg gratings to confirm computational predictions which will inform an iterative design process of optimising the ECL for eventual fabrication and characterisation.

ACKNOWLEDGMENTS

We would like to acknowledge the following Engineering and Physical Sciences Research Council (EPSRC) grants for their support: EP/S022139/1, the Centre for Doctoral Training in Connected Electronic and Photonic Systems and EP/T028475/1, "QUantum Dot on Silicon systems for communications, information processing and sensing (QUDOS)".

REFERENCES

[1] Chen, S., Li, W., Wu, J., Jiang, Q., Tang, M., Shutts, S., Elliott, S. N., Sobiesierski, A., Seeds, A. J., Ross, I., et al., "Electrically pumped continuous-wave III–V quantum dot lasers on silicon," *Nature Photonics* **10**(5), 307–311 (2016).

[2] Chen, S., Liao, M., Tang, M., Wu, J., Martin, M., Baron, T., Seeds, A., and Liu, H., "Electrically pumped continuous-wave 1.3 μm InAs/GaAs quantum dot lasers monolithically grown on on-axis Si (001) substrates," *Optics Express* **25**(5), 4632–4639 (2017).

[3] Shang, C., Hughes, E., Wan, Y., Dumont, M., Koscica, R., Selvidge, J., Herrick, R., Gossard, A. C., Mukherjee, K., and Bowers, J. E., "High-temperature reliable quantum-dot lasers on Si with misfit and threading dislocation filters," *Optica* **8**(5), 749–754 (2021).

[4] Yang, J., Li, K., Jia, H., Deng, H., Yu, X., Jurczak, P., Park, J.-S., Pan, S., Li, W., Chen, S., et al., "Low threading dislocation density and antiphase boundary free GaAs epitaxially grown on on-axis Si (001) substrates," *Nanoscale* **14**(46), 17247–17253 (2022).

[5] Bucio, T. D., Khokhar, A. Z., Lacava, C., Stankovic, S., Mashanovich, G. Z., Petropoulos, P., and Gardes, F. Y., "Material and optical properties of low-temperature NH_3-free PECVD SiNx layers for photonic applications," *Journal of Physics D: Applied Physics* **50**(2), 025106 (2016).

[6] Skandalos, I., Rutirawut, T., Domínguez Bucio, T., Hou, Y., Noori, Y., Tang, M., Chen, S., Liu, H., and Gardes, F. Y., "Monolithic III-V/SiN co-integration through a butt-coupling scheme towards O-band applications," (2022).

[7] Deng, H., Yang, J., Jia, H., Tang, M., Maglio, B., Jarvis, L., Shutts, S., Smowton, P. M., Chen, S., Seeds, A., et al., "Si-based 1.3 μm InAs/GaAs QD lasers," in [*2022 IEEE Photonics Conference (IPC)*], 1–2, IEEE (2022).

[8] Streifer, W., Scifres, D., and Burnham, R., "Coupled wave analysis of DFB and DBR lasers," *IEEE Journal of Quantum Electronics* **13**(4), 134–141 (1977).

[9] Kunii, T. and Matsui, Y., "Narrow spectral linewidth semiconductor lasers," *Optical and quantum electronics* **24**, 719–735 (1992).